Simulation of Subantarctic Mode and Antarctic Intermediate Waters in Climate Models

Article *in* Journal of Climate · October 2007

DOI: 10.1175/JCLI4295.1

2 authors:

Bernadette Sloyan
The Commonwealth Scientific and Indus…
67 PUBLICATIONS **1,564** CITATIONS

SEE PROFILE

Igor Kamenkovich
University of Miami
61 PUBLICATIONS **1,679** CITATIONS

SEE PROFILE

Simulation of Subantarctic Mode and Antarctic Intermediate Waters in Climate Models

BERNADETTE M. SLOYAN

Wealth from Oceans Flagship, and CSIRO Marine and Atmospheric Research, Hobart, Tasmania, Australia

IGOR V. KAMENKOVICH

University of Washington, Seattle, Washington

(Manuscript received 3 October 2006, in final form 25 January 2007)

ABSTRACT

The Southern Ocean's Subantarctic Mode Water (SAMW) and Antarctic Intermediate Water (AAIW) are two globally significant upper-ocean water masses that circulate in all Southern Hemisphere subtropical gyres and cross the equator to enter the North Pacific and North Atlantic Oceans. Simulations of SAMW and AAIW for the twentieth century in eight climate models [GFDL-CM2.1, CCSM3, CNRM-CM3, MIROC3.2(medres), MIROC3.2(hires), MRI-CGCM2.3.2, CSIRO-Mk3.0, and UKMO-HadCM3] that provided their output in support of the Intergovernmental Panel on Climate Change's Fourth Assessment Report (IPCC AR4) have been compared to the Commonwealth Scientific and Industrial Research Organisation (CSIRO) Atlas of Regional Seas. The climate models, except for UKMO-HadCM3, CSIRO-Mk3.0, and MRI-CGCM2.3.2, provide a reasonable simulation of SAMW and AAIW isopycnal temperature and salinity in the Southern Ocean. Many models simulate the potential vorticity minimum layer and salinity minimum layer of SAMW and AAIW, respectively. However, the simulated SAMW layer is generally thinner and at lighter densities than observed. All climate models display a limited equatorward extension of SAMW and AAIW north of the Antarctic Circumpolar Current. Errors in the simulation of SAMW and AAIW property characteristics are likely to be due to a combination of many errors in the climate models, including simulation of wind and buoyancy forcing, inadequate representation of subgrid-scale mixing processes in the Southern Ocean, and midlatitude diapycnal mixing parameterizations.

1. Introduction

The Southern Ocean's Subantarctic Mode Water (SAMW) and Antarctic Intermediate Water (AAIW) are two globally significant upper-ocean water masses that circulate in all of the Southern Hemisphere subtropical gyres and cross the equator to enter the North Pacific and North Atlantic Oceans. They are important components of the ocean heat and freshwater transport. SAMW and AAIW ventilate and resupply nutrients to the upper ocean, maintaining a substantial proportion of the global primary production (Sarmiento et al. 2004). They are components of the interbasin circulation associated with the Indonesian Throughflow (Schmitz 1996; Gordon 2001; Sloyan and Rintoul 2001a) and set the pycnocline structure in all Southern Hemisphere subtropical oceans. The export of North Atlantic Deep Water (NADW) into the Southern Ocean is largely balanced by northward transport of SAMW and AAIW (Gordon 1986; Rintoul 1991; Saunders and King 1995; Sloyan and Rintoul 2001a; Treguier et al. 2003). Here we analyze simulations of SAMW and AAIW for the twentieth century in eight climate models that provided their output in support of the Intergovernmental Panel on Climate Change's Fourth Assessment Report (IPCC AR4). Observation–model and model–model comparisons will assist in identifying model biases, incomplete understanding of ocean dynamics, and inadequate observations for complete validation of models. A greater understanding of present-day biases in climate model simulation of SAMW and AAIW will provide important knowledge in the assessment of the impact of changes in these water masses on climate under IPCC forcing scenarios.

SAMW and AAIW are formed near the Subantarctic

Corresponding author address: Bernadette Sloyan, CSIRO Marine and Atmospheric Research, GPO Box 1538, Hobart, Tasmania 7001, Australia.
E-mail: bernadette.sloyan@csiro.au

DOI: 10.1175/JCLI4295.1

Front (SAF), which is the northernmost front of the Antarctic Circumpolar Current (ACC), predominantly in the Indian and Pacific sectors of the Southern Ocean. It appears that the formation of SAMW and AAIW and their characteristic properties are effected by air–sea exchanges of heat and freshwater and Ekman transport over the region of layer outcrop (McCartney 1982; Bindoff and McDougall 1994; Ribbe 1999; Santoso and England 2004), variations in the wind stress (Ribbe 2001; Rintoul and England 2002), subsurface cross-frontal mixing (Piola and Georgi 1982; Piola and Gordon 1989), and lateral advection (McCartney 1982). Processes involved in SAMW and AAIW formation are still poorly understood, and the relative importance of any one process in determining the formation rate of SAMW and AAIW and their characteristic properties is yet to be determined.

Climate studies have observed decadal differences in the temperature and salinity of SAMW and AAIW in the subtropical pycnocline and Southern Ocean (Bindoff and Church 1992; Johnson and Orsi 1997; Wong et al. 1999; Bindoff and McDougall 2000; Gille 2002; Bryden et al. 2003). Changes in density are communicated between the Southern Ocean and low latitudes within 10–20 years through the process of baroclinic adjustment following the boundary layer path (Goodman 2001). These decadal differences have been linked to anthropogenic climate change (Banks and Wood 2002; Banks and Bindoff 2003). Arbic and Owens (2001) suggest that warming trends in the North Atlantic can be in part traced to the changes in the Southern Ocean regions. Changes in the surface density of the Southern Ocean may affect the overturning of NADW and the depth of the pycnocline in the Atlantic (Wang et al. 1999; Keeling 2002), and SAMW and AAIW play a central role in both the processes (Saenko et al. 2003; Kamenkovich and Sarachik 2004).

This study evaluates the climate model simulation of the properties and transport of SAMW and AAIW in the Atlantic, Indian, and Pacific Oceans and the adjacent Southern Ocean region for the present-day climate. Details of the observational climatology and climate models are provided in section 2. Simulations of SAMW and AAIW properties (temperature and salinity, potential vorticity, and salinity minimum) and upper-ocean stratification are compared among the models and to observational data in sections 3 and 4. Analysis of the volume and heat transport of SAMW and AAIW across the subtropical gyres between the climate model simulations and a data-based inverse model are given in section 5. The discussion (section 6) and conclusions (section 7) close the paper.

2. Observations, inverse model, and climate model details

a. Observational climatology

In this study we use the Commonwealth Scientific and Industrial Research Organisation (CSIRO) Atlas of Regional Seas 2006 (CARS2006; available online at www.marine.csiro.au/~dunn/cars2006), which is a $0.5° \times 0.5°$ gridded climatology in the region from 70°S to 26°N, 0° to 360°E except that the northern boundary is 10°N in the Atlantic Ocean. Vertically the ocean is divided into 79 standard depths from the sea surface to 5500 m with 60 layers in the upper 1500 m.

Data in CARS2006 are derived from the National Ocean Data Center (NODC) World Ocean Atlas 2001 hydrographic data, the World Ocean Circulation Experiment (WOCE) hydrographic program, the CSIRO archive of Australian hydrography data, and Argo profiling floats. Data are screened for duplicates and bad positions, outliers to local temperature–salinity relations in density coordinates, and outliers of residuals to intermediate mappings. The data are interpolated onto a regular grid using a loess filter (Ridgway et al. 2002). Quadratics are fitted in horizontal and vertical coordinates with bathymetry-influenced weighting. Annual harmonics are simultaneously fitted down to 1000 m for temperature, salinity, and nutrient data. For temperature and salinity, where data density was much higher, semiannual harmonics are also fitted over the upper 1000 m. For every mapped point, an ellipse was calculated that provided 400 data points at that depth. Other points are used from one standard depth above and below, if their combined x–y radius, z distance, and bathymetry-weight distance fell within the 400-point horizontal radius (Dunn and Ridgway 2002).

In this study, monthly mean temperature and salinity properties and potential density between the sea surface and 1500 m (60 standard depth levels) are produced from the CARS2006 annual and semiannual harmonics. The CARS2006 monthly climatologies are mapped onto five potential density surfaces (σ_θ = 26.7, 26.9, 27.0, 27.2, 27.4, and 27.6 kg m^{-3}) that define the SAMW and AAIW water masses (Fig. 1). Seasonal climatologies [austral summer (December–February), austral autumn (March–May), austral winter (June–August), and austral spring (September–November)] of isopycnal depth, temperature and salinity, and potential vorticity are compared to climate model simulations of SAMW and AAIW (section 3). The CARS2006 isopycnal seasonal climatology is subsampled to individual climate model grids for comparison with each climate model.

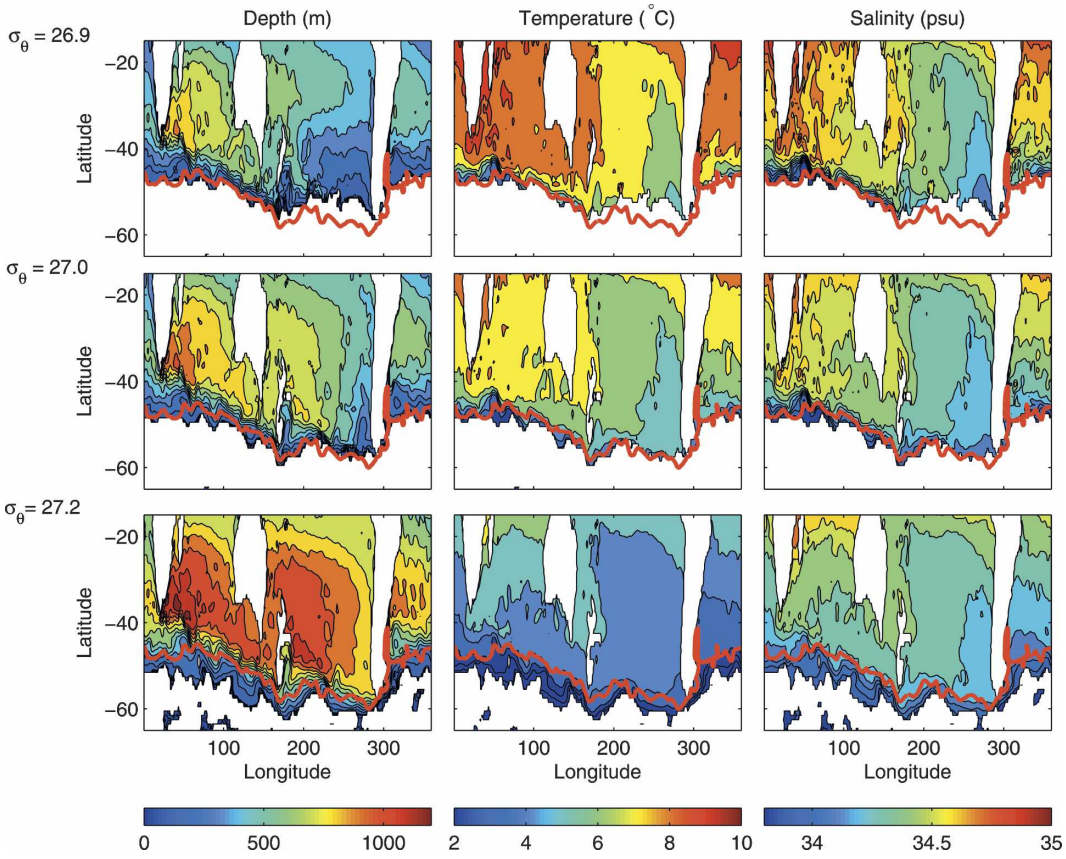

FIG. 1. Depth, temperature, and salinity distribution from CARS2006 for austral spring (September–November) on (top) σ_θ = 26.9 kg m^{-3}, (middle) 27.0 kg m^{-3}, and (bottom) 27.2 kg m^{-3}. These potential density surfaces are within SAMW, the boundary between SAMW and AAIW, and trace the AAIW salinity minimum, respectively. Also shown is the position of the Subantarctic Front (solid red) (from Orsi et al. 1995). Contour interval: depth 20 to 100 m, 100 to 1500 m, temperature 1°C, salinity 0.1 psu.

b. *Climate models*

The simulations of SAMW and AAIW are investigated in eight climate models (Table 1; details of IPCC climate models can be found online at www-pcmdi.llnl.gov/ipcc/about_ipcc.php). All oceanic components of these climate models, with the exception of the Model for Interdisciplinary Research on Climate 3.2, high-resolution version [MIROC3.2(hires)], employ a coarse longitudinal (x) resolution of 1°–2°. Latitudinal (y) resolution varies among the climate models. Most models have a latitudinal (y) resolution between 1° and 2° at mid and high latitudes, while surrounding the equator resolution increases to less than 0.5°. The exceptions are the CSIRO Mark version 3.0 (CSIRO-Mk3.0) and the Met Office Third Hadley Centre Coupled Ocean—Atmosphere GCM (UKMO-HadCM3) climate models, which maintain a constant y resolution over the entire model domain, and the Community Climate System Model, version 3 (CCSM3) and MIROC3.2(hires) models, which employ a fine meridional resolution throughout their model domain. The main difference between the medium-resolution MIROC 3.2 [MIROC3.2(medres)] and MIROC3.2(hires) climate models is the horizontal resolution. The vertical coordinate is either a z coordinate or hybrid z coordinate/σ coordinate with resolution of 40–50 levels [Geophysical Fluid Dynamics Laboratory Climate Model version 2.1 (GFDL-CM2.1), CCSM3, MIROC3.2(medres), and MIROC3.2(hires)] or 20–33 levels [Centre National de Recherches Météorologiques Coupled Global Climate Model, version 3 (CNRM-CM3), Meteorological Research Institute Coupled GCM version 2.3.2 (MRI-CGCM2.3.2), UKMO-HadCM3, and CSIRO-Mk3.0]. The climate models employ a variety of parameterizations to represent missing subgrid-scale processes. Unresolved heat and salt transports by mesoscale eddies are parameterized by the Gent–McWilliams scheme (Gent and McWilliams 1990); other parameterizations are also used by the models (Table 1). Flux

TABLE 1. Detail of the climate models considered in this study. National Oceanic and Atmospheric Administration (NOAA), National Center for Atmospheric Research (NCAR), Center for Climate System Research (CCSR, The University of Tokyo), National Institute for Environmental Studies (NIES), Frontier Research Center for Global Change (FRCGC), Japan Agency for Marine-Earth Science and Technology (JAMSTEC), k-profile parameterization (KPP), Gent–McWilliams mesoscale eddy parameterization (GM) (Gent and McWilliams 1990), Mellor–Yamada mixing scheme (MY) (Mellor and Yamada 1982), Price–Weller–Pinkel mixed layer parameterization (PWP) (Price et al. 1986), integer power vertical mixing (IP) (Wilson 2000), and Kraus–Turner (KT) (Kraus and Turner 1967). MIROC3.2(hires) is resampled for use in IPCC at coarser resolution.

Climate model	Institution	Horizontal resolution	Vertical resolution	Parameterized processes
GFDL-CM2.1	NOAA/GFDL	x: 1° y: 1°–0.33°	z: 50 levels	KPP; tidal mixing; GM
CCSM3	NCAR	x: 1.125° y: 0.53°–0.27°	z: 40 levels	KPP; GM
CNRM-CM3	CNRM	x: 2° y: 1.5°–0.5°	z: 31 levels	TKE; isopycnal diffusion
MIROC3.2 (hires)	CCSR/NIES FRCGC(JAMSTEC)	x: 0.28° y: 0.19°	z and σ: 47 levels	Biharmonic mixing; GM; MY
MIROC3.2 (medres)	CCSR/NIES FRCGC(JAMSTEC)	x: 1.4° y: 1.4°–0.56°	z and σ: 43 levels	Weak κ diffusion; GM; MY
MRI-CGCM2.3.2	MRI	x: 2.5° y: 2°–0.5°	z: 33 levels	GM; MY Horizontal diffusion
CSIRO- Mk3.0	CSIRO, Marine and Atmospheric Research	x: 1.87° y: 0.84°	z: 31 levels	GM; PWP IP mixing
UKMO-HadCM3	Hadley Centre for Climate Prediction	x: 1.25° y: 1.25°	z: 20 levels	GM; biharmonic mixing; KT

adjustments are not used in any of these climate models except for MRI-CGCM2.3.2.

Following the recommendation of the IPCC, we define the model mean climate as the 20-yr average (1981–2000) of the simulated climate of the twentieth century. The fact that the current generation of climate models can simulate the present-day climate without relying on flux adjustments is a remarkable achievement. However, some systematic drift of oceanic variables still occurs in the models' control simulations. The model drift is mainly a result of a mismatch between the atmosphere–ocean exchanges of heat, water, and momentum and oceanic transports of these quantities (Kamenkovich et al. 2002). There are two main implications of this drift for our analysis. First, systematic drift during spinup of these models results in deviations of oceanic variables from their initial values. As most oceanic models are initialized from observational data, the drift may be a significant cause of any apparent disagreement between the climate-model simulated fields and observations. Second, if any given model continues to exhibit a significant drift during the twentieth and twenty-first-century simulations, the definition of the mean climate becomes ambiguous. It is possible to correct the models for this unphysical systematic drift by removing the drift magnitude, calculated from the control simulations, from all simulated fields. However, here we report the magnitude of the drift over the 110-yr control simulation for each model but do not remove the drift from the models' twentieth-century mean climate (Figs. 2 and 3). North of 50°S model temperature and salinity drift in the upper 1500 m of the water column is generally less than 0.6°C and 0.1 psu.

Potential density is calculated from the model temperature and salinity fields. The climate models' mean seasonal simulations of isopycnal depth, temperature, and salinity are determined for five isopycnal surfaces. The ensemble root-mean-square (rms) error for the five isopycnal surfaces in the climate model relative to CARS2006 are calculated, and the potential vorticity and salinity minimum layers traced north of the ACC.

Finally, for a subset of the climate models, we calculate the meridional volume and temperature transport of SAMW and AAIW across 12°S in the Atlantic and 32°S in the Indian and Pacific Oceans. In the climate model we define similar "sections" to those used in the observational-based inverse model of Sloyan and Rintoul (2001a) to compare meridional volume and temperature transport among the climate models and with the inverse model.

3. Simulation of SAMW and AAIW properties

Recently ventilated SAMW and AAIW enters the Indian and Pacific Oceans in a broad region east of the western boundary currents and circulates within the wind-driven subtropical gyres (Fig. 1). In austral spring

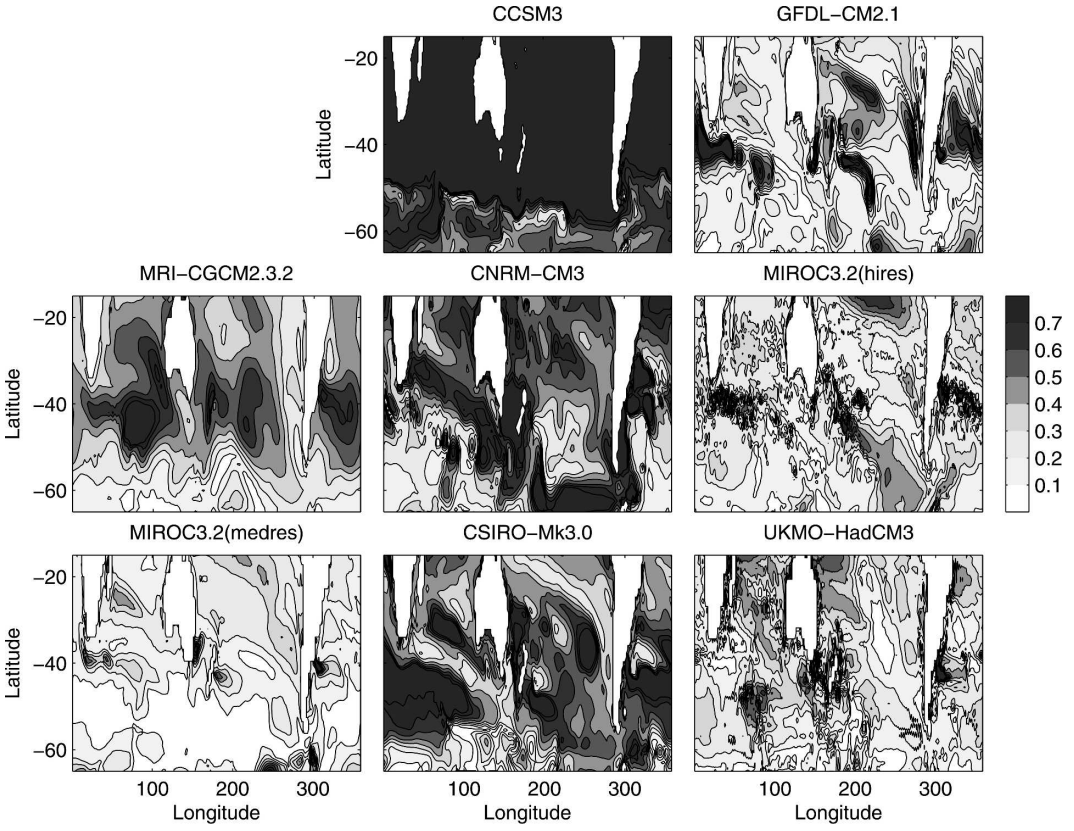

FIG. 2. Magnitude of the temperature drift [°C (110 yr)$^{-1}$] over the upper ocean (0 to ≈ 1500 m) for the eight climate models.

the isopycnal surfaces that define SAMW and AAIW outcrop near the SAF; however, circumpolarly, there is some variation of the outcrop density coincident with the front. In the Indian sector of the Southern Ocean the SAMW isopycnal ($26.7 \leq \sigma_\theta \leq 27.0$ kg m^{-3}) outcrop is nearly coincident with the SAF, while $\sigma_\theta \geq 27.0$ kg m^{-3} outcrops south of the SAF with surface temperature and salinity properties of Antarctic Surface Water (Fig. 1). East of New Zealand (~160°E), $\sigma_\theta = 26.9$ kg m^{-3} outcrops north of the SAF, and in the eastward direction toward Drake Passage the SAF is increasingly coincident with the outcrop position of $\sigma_\theta = 27.0$ kg m^{-3}. The coldest and freshest varieties of SAMW and AAIW enter the eastern Pacific Ocean adjacent to South America or flow through Drake Passage with the ACC. The isopycnal property distribution of SAMW and AAIW from CARS2006 agrees with previous studies (McCartney 1977, 1982).

In this section we compare the austral spring simulation of SAMW and AAIW isopycnal depth, temperature and salinity, and depth and latitudinal extent of the SAMW potential vorticity minimum and AAIW salinity minimum among the eight climate models relative to CARS2006. The CARS2006 climatology is interpolated to the climate model horizontal and vertical resolution (Table 1). Similar to Gnanadesikan et al. (2006), ensemble rms isopycnal property errors of model-simulated SAMW and AAIW, relative to CARS2006, are compared among the eight climate models. Our analysis of the climate models will focus on the region north of the ACC to 15°S.

a. Isopycnal temperature and salinity

SAMW and AAIW rms isopycnal temperature and salinity errors relative to CARS2006 show that a number of the climate models simulate the isopycnal temperature and salinity of SAMW and AAIW to within ±2°C and ±0.3 psu (Figs. 4 and 5). Regional differences in rms SAMW and AAIW isopycnal temperature and salinity errors are seen within each climate model and among the climate models. Most of the climate models have their smallest rms temperature and salinity errors in the eastern Pacific between the ACC and 20°S. However, the amplitude of the error differs among the climate models.

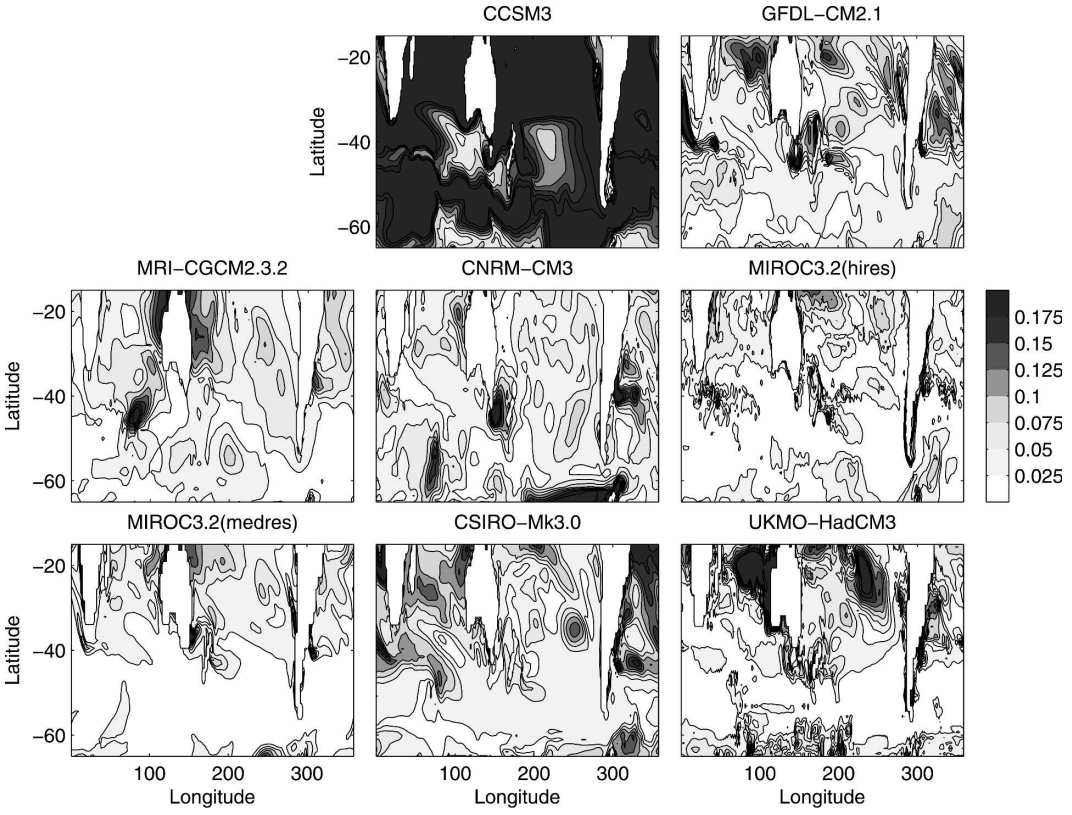

FIG. 3. As in Fig. 2, except for salinity drift [psu (110 yr)$^{-1}$].

The UKMO-HadCM3 and MRI-CGCM2.3.2 have the largest isopycnal temperature and salinity errors. Significant errors are seen in the Indian Ocean in both climate models. In the GFDL-CM2.1 and CSIRO-Mk3.0 models the eastern Pacific errors are less than ±0.5°C and ±0.1 psu. In both of these climate models and in CCSM3 the isopycnal property error increases westward of 200°E, reaching a maximum at the western boundary of the Pacific Ocean adjacent to Australia and New Zealand. In the Pacific Ocean, the MIROC3.2(hires), MIROC3.2(medres), and CNRM-CM3 models have a similar magnitude of property error across the Pacific basin, with small property errors in the extratropical region north of 20°S and along the western boundary north of 30°S. In all of these models [CCSM3, GFDL-CM2.1, CNRM-CM3, MIROC3.2 (hires, medres), and CSIRO-Mk3.0] the isopycnal temperature and salinity errors increase in the Indian Ocean north of ~45°S, in the Agulhas retroflection, and in the Falkland–Brazil confluence region. The largest errors are found south of Australia and in the eastern and central Indian Ocean where recently ventilated SAMW enters the subtropical gyre (Sloyan and Rintoul 2001a).

b. *Isopycnal depth*

The climate model isopycnal depth errors are broadly classified into three major patterns: hemispheric, basin, and those related to the position of the ACC and/or simulation of boundary (west and east) features (Fig. 6). The MRI-CGCM2.3.2, UKMO-HadCM3, and CNRM-CM3 models display large-scale hemispheric depth errors greater than ±250 m equatorward of the ACC.

The second pattern of isopycnal depth error is associated with the simulation of the stratification in individual basins. GFDL-CM2.1 and MIROC3.2(hires, medres) all have their largest rms isopycnal depth error in the Pacific subtropical gyre and southeastern Indian Ocean. South and east of Western Australia the isopycnal rms depth error is coincident with the formation site of southeastern Indian SAMW (Hanawa and Talley 2001). Isopycnal depth errors in this region are also seen in CCSM3 and CSIRO-Mk3.0.

The final pattern of isopycnal depth errors is associated with the simulation of the position and structure of the ACC in the climate models and with representation of the vertical distribution of density at the western and

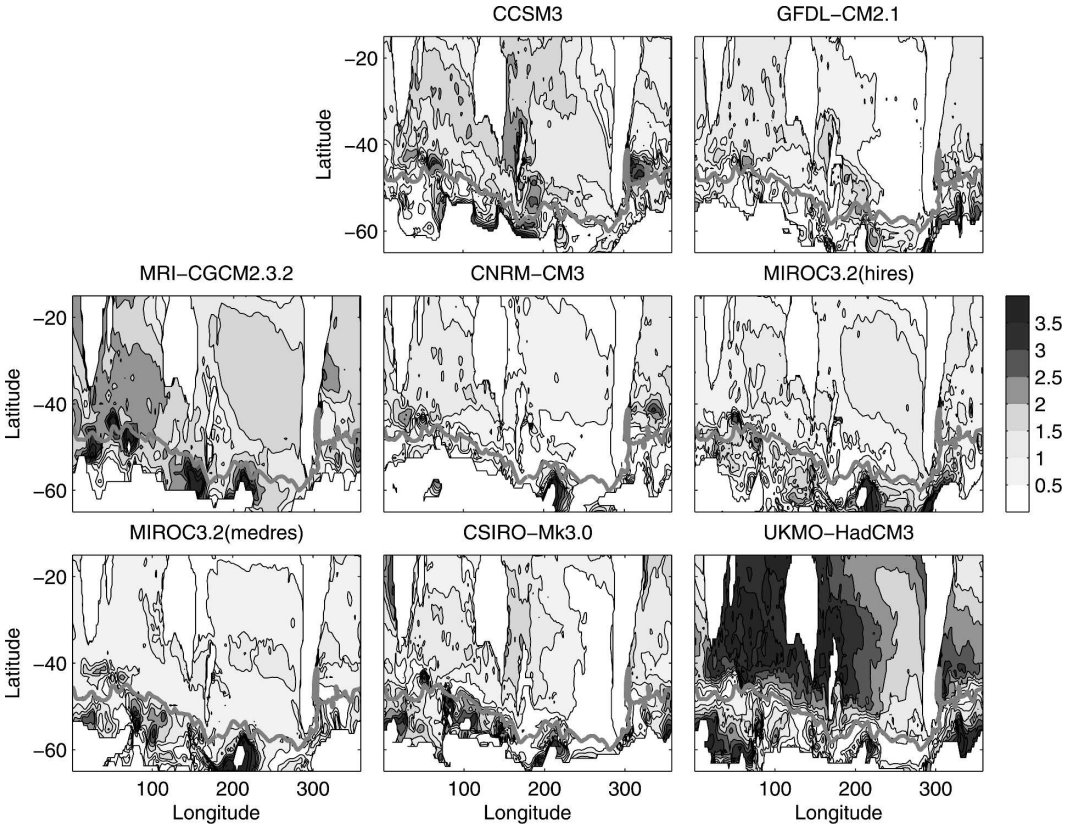

FIG. 4. Rms ensemble isopycnal temperature error (°C) on σ_θ = 26.7, 26.9, 27.0, 27.2, and 27.4 kg m^{-3} for austral spring relative to CARS2006. The potential density surfaces define SAMW and AAIW in the observational climatology. Also shown is the position of the Subantarctic Front (solid gray) (from Orsi et al. 1995).

eastern boundaries of the Atlantic, Indian, and Pacific basins. Errors in the simulation of the ACC position and structure are seen in all models (Fig. 6), with CCSM3, GFDL-CM2.1, and MIROC3.2(hires) models best simulating the ACC density structure. In the Southern Ocean, the CCSM3, GFDL-CM2.1, and MIROC3.2(hires) largest isopycnal depth errors are found surrounding topographical barriers along the ACC pathway (90°E–Kerguelen Plateau, 170°E–Macquarie Ridge and Campbell Plateau, and 300°E–Drake Passage and Falkland Plateau). The climate models also display large isopycnal depth errors at the eastern boundaries of the Pacific and Indian Oceans, at the Pacific Ocean western boundary adjacent Australia and New Zealand, within the Agulhas Current retroflection region south of Africa, and in the Falkland–Brazil confluence region in the Atlantic Ocean. SAMW and AAIW circulate in the subtropical gyres below the thermocline. In the subtropical and tropical regions, errors in the depth of the isopycnal surfaces are indicative of errors in the upper-ocean temperature distribution in the climate models. The depth error of SAMW and AAIW water masses within the subtropical ocean is significant given that these water masses supply nutrients to the surface ocean via vertical mixing that drive primary production in these regions. Correct ocean dynamics is vital for assessing the affect of possible future climate variability and change of SAMW and AAIW on the marine ecosystem and the ocean carbon cycle.

c. *SAMW potential vorticity minimum layer*

Austral winter and early spring convection results in the formation of SAMW, which is identified by a potential vorticity minimum layer on the equatorward side of the SAF (Figs. 7 and 8). In the Indian Ocean, SAMW ($26.7 \leq \sigma_\theta \leq 26.9$ kg m^{-3}) extends equatorward from the SAF (Fig. 7). In the Indian Ocean all models produce a potential vorticity minimum layer on the northern boundary of the model ACC; however, in most models, apart from CSIRO-Mk3.0, the potential vorticity minimum is not produced at the observed density. The climate model potential vorticity minimum layer is also generally thinner than observed, except for MIROC3.2(medres) and CSIRO-Mk3.0. The thickness

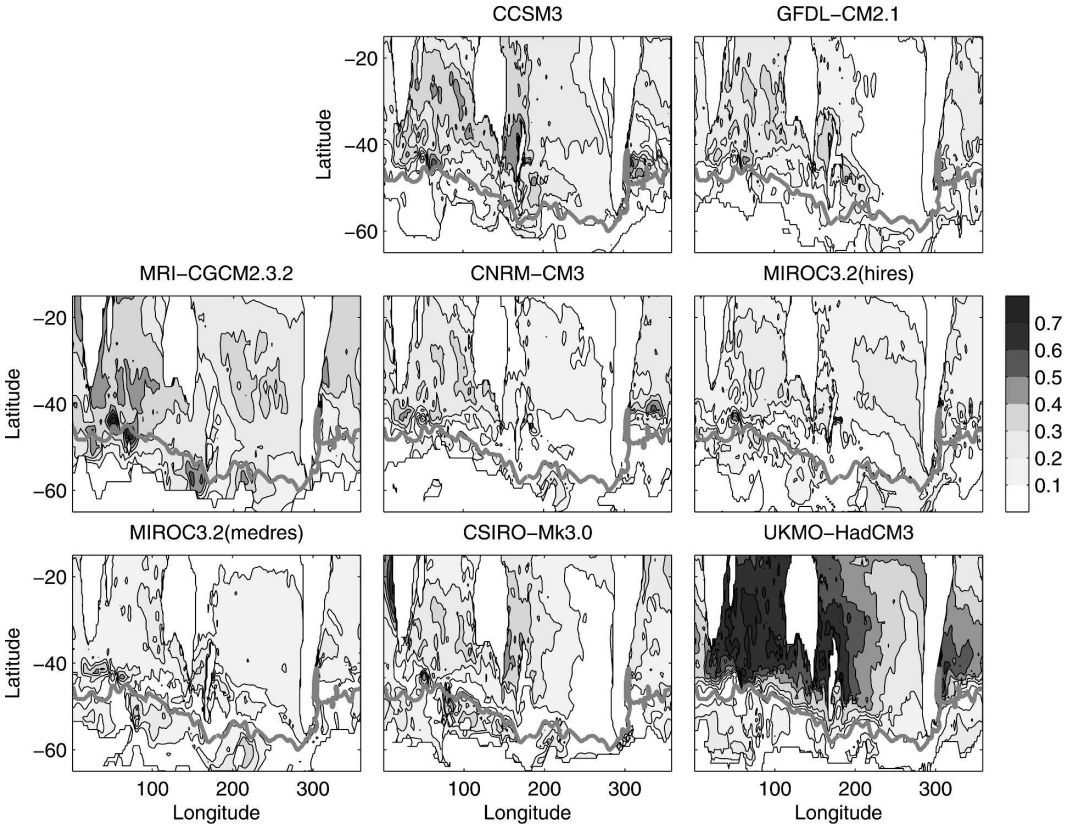

FIG. 5. As in Fig. 4, except for ensemble isopycnal salinity error (psu).

of the MIROC3.2(medres) low potential vorticity layer is well simulated with respect to observations, while the CSIRO-Mk3.0 low potential vorticity layer is too thick, extending to approximately 1000 m. All climate models show a limited latitudinal extent of the potential vorticity minimum layer that only extends northward to about 30°S.

In the eastern Pacific Ocean the potential vorticity minimum layer is associated with both SAMW and AAIW ($26.9 \leq \sigma_\theta \leq 27.2$ kg m^{-3}) and is coincident with the low salinity layer (Fig. 10). Most climate models have a potential vorticity minimum layer in the eastern Pacific, which is generally associated with less dense water than observed. However, there are clear differences among the models regarding how well they simulate the equatorward extension and depth of the potential vorticity minimum with respect to observations. The GFDL-CM2.1 and MIROC3.2(medres) models simulate a potential vorticity minimum layer that has a similar shape and latitudinal extent as that observed. We note that while CSIRO-Mk3.0 simulates the potential vorticity minimum at the correct density and associated pycnostad, the potential vorticity minimum layer extends much deeper than observed.

d. AAIW salinity minimum layer

AAIW penetration into the subtropical gyres is identified by a subsurface salinity minimum layer that extends equatorward from the SAF at approximately 1000 m in the Indian Ocean and 600 m in the Pacific Ocean (Figs. 9 and 10). AAIW in the Indian Ocean is defined by a distinct subsurface salinity minimum that is nearly coincident with $\sigma_\theta = 27.2$ kg m^{-3}, while in the eastern Pacific Ocean the AAIW salinity minimum is broadly defined between $27.0 \leq \sigma_\theta \leq 27.2$ kg m^{-3}.

In the eastern Indian Ocean all climate models simulate a salinity minimum layer south of 40°S. The MRI-CGCM2.3.2 salinity minimum layer is saltier than observed, too shallow, and has a very limited latitudinal extent north of the ACC. That of UKMO-HadCM3 is too fresh with salinity ≤33.5 psu extending from the sea surface to 200 m between 42° and 61°S. In contrast, CSIRO-Mk3.0 has an AAIW salinity minimum layer that is saltier and deeper than observed, while the CNRM-CM3 AAIW salinity minimum is too salty south of 40°S. The CCSM3, GFDL-CM2.1, and MIROC3.2(hires, medres) best simulate the AAIW salinity minimum between the ACC and 40°S. In these

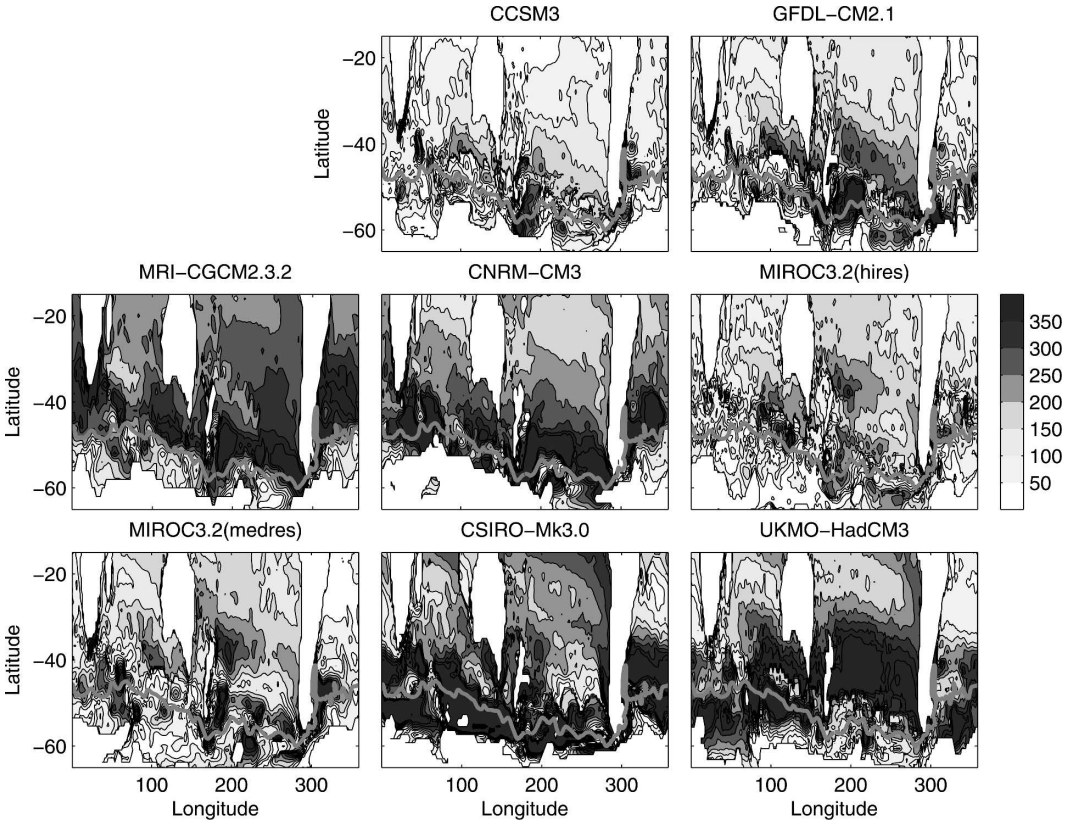

FIG. 6. As in Fig. 4, except for ensemble isopycnal depth error (m).

climate models the simulated AAIW salinity minimum is at the observed density below 600 m. North of 40°S the salinity minimum layer in the CCSM3, GFDL-CM2.1, and MIROC3.2(hires) models becomes less distinct between the overlying and underlying water masses.

In the eastern Pacific Ocean a thick low salinity tongue is observed south of 35°S from the sea surface to 1000 m and it is coincident with the potential vorticity minimum layer (Fig. 8). The GFDL-CM2.1 best simulates the salinity of the upper 1000 m of the eastern Pacific and latitudinal extent of the low salinity layer when compared to observations and other climate models. CNRM-CM3 and MIROC3.2(hires, medres) all simulate the salinity of SAMW and AAIW reasonably well south of 45°S, but in general the low salinity layer is shallower than observed and has limited equatorward penetration into the subtropical Pacific Ocean. The UKMO-HadCM3 has salinity $\leq$33.5 psu extending from the sea surface to 400 m between 57° and 30°S, while CCSM3 also has salinities in the upper 400 m that are fresher than observed (Fig. 10). In contrast, that of MRI-CGCM2.3.2 is saltier than observed. Throughout much of the upper 1400 m the CSIRO-Mk3.0 salinity is fresher than observed.

4. Evaluation of SAMW and AAIW property simulation in climate models

Property simulations, relative to CARS2006, of SAMW and AAIW vary among the climate models and spatially within the climate models. All climate models produce a potential vorticity minimum and salinity minimum layer associated with SAMW and AAIW, respectively. However, among the climate models there is considerable variability in density, depth, and latitudinal extent of these features. In this study our benchmark of how well the climate models simulate SAMW and AAIW is small rms isopycnal temperature and salinity errors, production of an appropriate thick potential vorticity minimum and salinity minimum layer within the observed density range, and equatorward extension of these features from the northern boundary of the ACC. We have chosen these properties as they are synonymous with the formation and circulation pathway of SAMW and AAIW. Other studies may define different criteria for assessing the climate model simulation of these water masses and therefore reach different conclusions regarding the "goodness" of a model's simulation of these water masses.

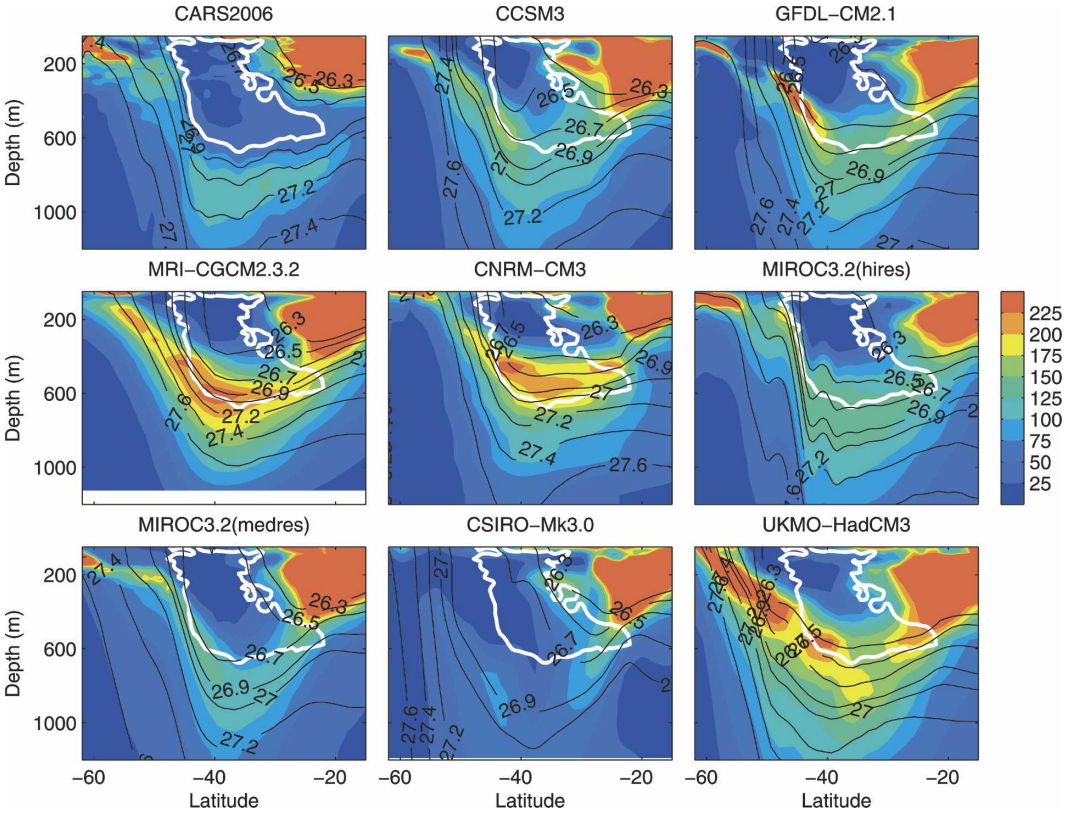

FIG. 7. Austral spring distribution of potential vorticity [$\times 10^{-14}$ (cm s)$^{-1}$] in the eastern Indian Ocean (100°E) from CARS2006 and eight climate models. The depth and latitudinal extent of observed SAMW potential vorticity minimum layer [$\leq 50 \times 10^{-14}$ (cm s)$^{-1}$, bold white] is overlain on climate model potential vorticity distribution. Also shown is the distribution of potential density (solid black).

The UKMO-HadCM3 model appears to have a very active hydrological cycle with excess precipitation over the Southern Ocean and excess evaporation over low latitudes (Pardaens et al. 2003). The excess precipitation over the Southern Ocean results in the model producing extremely fresh AAIW that is both too shallow and too light. UKMO-HadCM3 has the largest rms isopycnal salinity errors (≥0.4 psu) among the climate models. Pardaens et al. (2003) suggest that the overly active hydrological cycle in UKMO-HadCM3 is the result of a too strong Hadley and Walker circulation and an overestimate of poleward freshwater flux. The effect on the ocean component of the climate model is increased stratification in the upper ocean, which appears to limit the development of deep winter mixing surrounding the model ACC and convection equatorward of the front.

The MRI-CGCM2.3.2 model has significant problems simulating the formation of SAMW and AAIW in the Southern Ocean and the northward penetration of these water masses into the adjacent subtropical gyres. The MRI-CGCM2.3.2 salinity is too salty below 600 m and no salinity minimum layer is found north of 40°S in the Indian Ocean. The model does simulate a potential vorticity minimum in the Indian sector of the Southern Ocean but this minimum does not extend beyond 30°S. Errors in the simulation of SAMW and AAIW in MRI-CGCM2.3.2 may have many causes and could be related to inconsistency between the coupling of the ocean and atmosphere.

In the Southern Ocean, the CSIRO-Mk3.0 model simulates isopycnal surfaces that are much deeper than observed with an rms error relative to CARS2006 of ≥400 m. This model has excessive convection in the Southern Ocean (S. O'Farrell and A. Hirst 2006, personal communication). The potential vorticity minimum of SAMW in the Indian and Pacific sector of the Southern Ocean, although at the correct density, extends below 800 m and does not penetrate north of 40°S, while the AAIW salinity minimum lies below 1200 m in the Southern Ocean. Therefore, although the magnitude of the isopycnal property errors is similar in GFDL-CM2.1, the large rms error of the depth of the SAMW and AAIW isopycnal surfaces north of the SAF

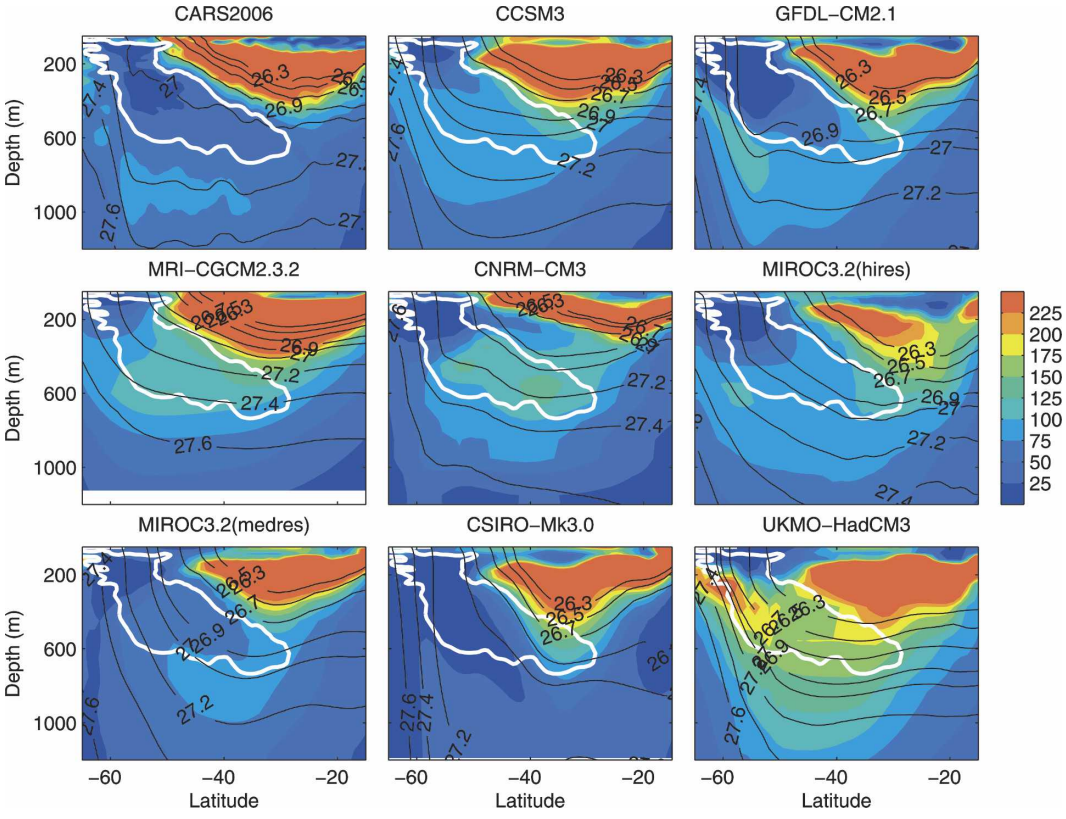

FIG. 8. As in Fig. 7, except for the eastern Pacific Ocean (90°W).

result in SAMW and AAIW being too deep in the adjacent subtropical basins.

The GFDL-CM2.1, CCSM3, CNRM-CM3, and MIROC3.2(medres) models best simulate the properties of SAMW and AAIW. The differences between MIROC3.2(medres) and MIROC3.2(hires) are small; however, differences between the model rms errors suggest that the MIROC3.2(medres) simulation of SAMW and AAIW is slightly better than for the higher-resolution model. In these models the SAMW potential vorticity minimum layer near the ACC is reasonably well simulated with respect to its observed position and depth. Most models capture the equatorward extension of the potential vorticity minimum into the eastern Pacific but not into the eastern Indian Ocean. In all four models the SAMW pycnostad is produced at lighter densities than observed. This error results in the large rms isopycnal depth errors in all models on the equatorward side of the ACC. In the Indian sector of the Southern Ocean the subducted AAIW salinity minimum is at the correct density and depth in GFDL-CM2.1 and CCSM3. In MIROC3.2(medres) the salinity minimum is too deep and at a denser isopycnal surface than observed, and in CNRM-CM3 the salinity minimum is too shallow but at the correct density. AAIW in the CCSM3, GFDL-CM2.1, and CNRM-CM3 models is too thick north of 40°S, clearly suggesting that midlatitude diapycnal mixing is overestimated in these models. All models adequately simulate the thick low-salinity layer of SAMW and AAIW in the eastern Pacific and its equatorward extension into the eastern Pacific Ocean.

5. SAMW and AAIW property transport into the Pacific and Indian Oceans

Following definitions used by Sloyan and Rintoul (2001b), we compute the climate-model simulated SAMW and AAIW volume and temperature transport between neutral densities $26.0 \leq \gamma^n \leq 27.4$ kg m^{-3}, for the GFDL-CM2.1, CCSM3, CNRM-CM3, and MIROC3.2(medres) models. The $\gamma^n = 26.0$ kg m^{-3} neutral density is the boundary between SAMW and overlying thermocline water in the subtropical gyres, while $\gamma^n = 27.4$ kg m^{-3} is the boundary between AAIW and Upper Circumpolar Deep Water in the Southern Ocean, and Indian Deep Water and Pacific Deep Water and NADW in the subtropical gyres. The broad density definition employed by Sloyan and Rin-

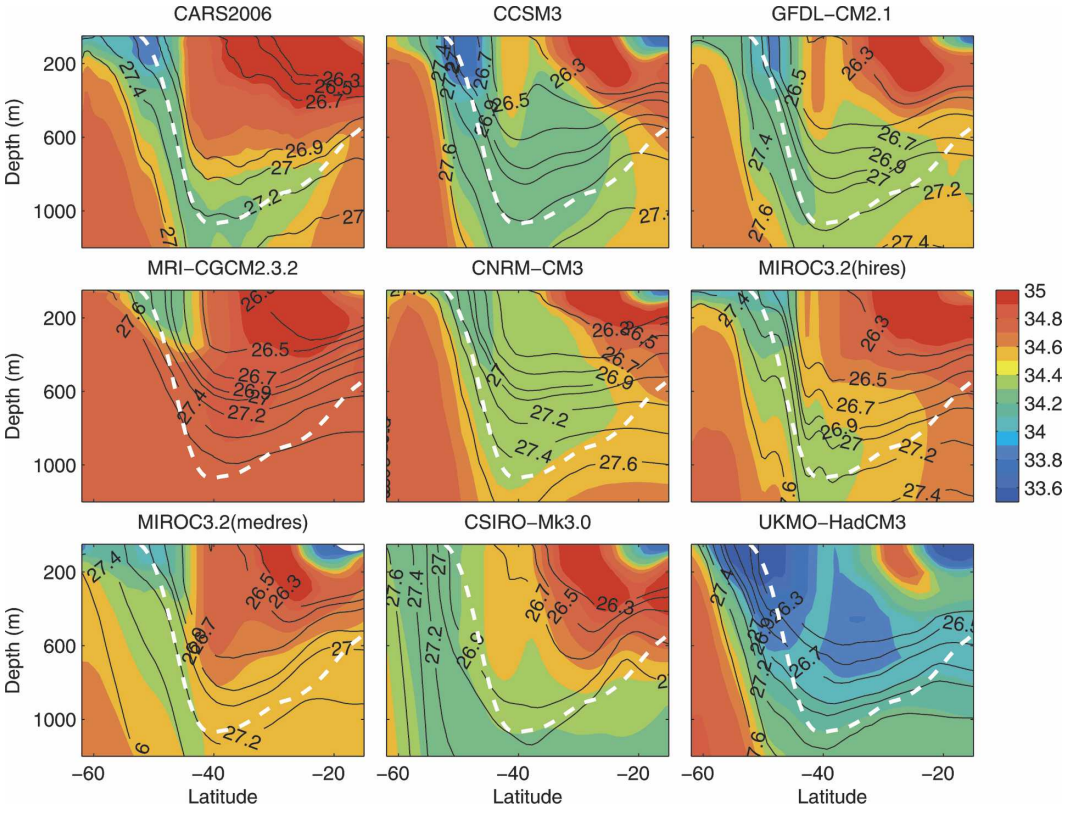

FIG. 9. Austral spring distribution of salinity (psu) in the eastern Indian Ocean (100°E) from CARS2006 and eight climate models. The depth and latitudinal extent of observed AAIW salinity minimum (bold white) is overlain on climate model salinity distribution. Also shown is the distribution of potential density (solid black).

toul results in most models producing the SAMW potential vorticity within this neutral density range. The definition of the SAMW and AAIW boundaries based on the density (neutral and/or potential) is not unique, and the lower boundary of AAIW may also be defined at the salinity minimum core. We choose a neutral density-based definition because our objective is to compare the observation-based inverse model SAMW and AAIW volume and temperature transport estimates with climate-model simulated transports. The GFDL-CM2.1, CCSM3, CNRM-CM3, and MIROC3.2 (medres) models best simulate the depth and isopycnal horizon of the AAIW salinity minimum as it enters the subtropical gyre. Therefore, the density definition of SAMW and AAIW used by Sloyan and Rintoul (2001b) is consistent with the simulated water masses in these four models.

The calculation of neutral density is, however, only accurate as long as the climate-model simulated fields are not too different from the temperature and salinity observed climatology. GFDL-CM2.1, CCSM3, and MIROC3.2(medres) best simulated the isopycnal temperature and salinity of SAMW and AAIW. CNRM-CM3 has larger rms isopycnal property errors but was included because its AAIW salinity and density are in reasonable agreement with observations. Monthly means of temperature, salinity, and meridional velocities are used to compute neutral density, SAMW/AAIW layer thickness, and meridional property transports. Our analysis will be restricted to the advective heat fluxes and will not include the heat fluxes due to mesoscale eddies and parameterized by diffusion in coarse-resolution climate models owing to difficulties in their computation from the monthly mean temperatures and densities.

To investigate the influence of the defined boundaries of the water masses, we carry out some additional analysis. First, we combine the surface and thermocline water layers with the SAMW and AAIW layer and calculate the basin-integrated volume transports (not shown), eliminating the influence of the position of the upper boundary of SAMW and AAIW. Second, we divide the volume transports in the SAMW and AAIW layer by its thickness. The resulting average velocities (not shown) by the southward western boundary currents and the northward interior flows are generally

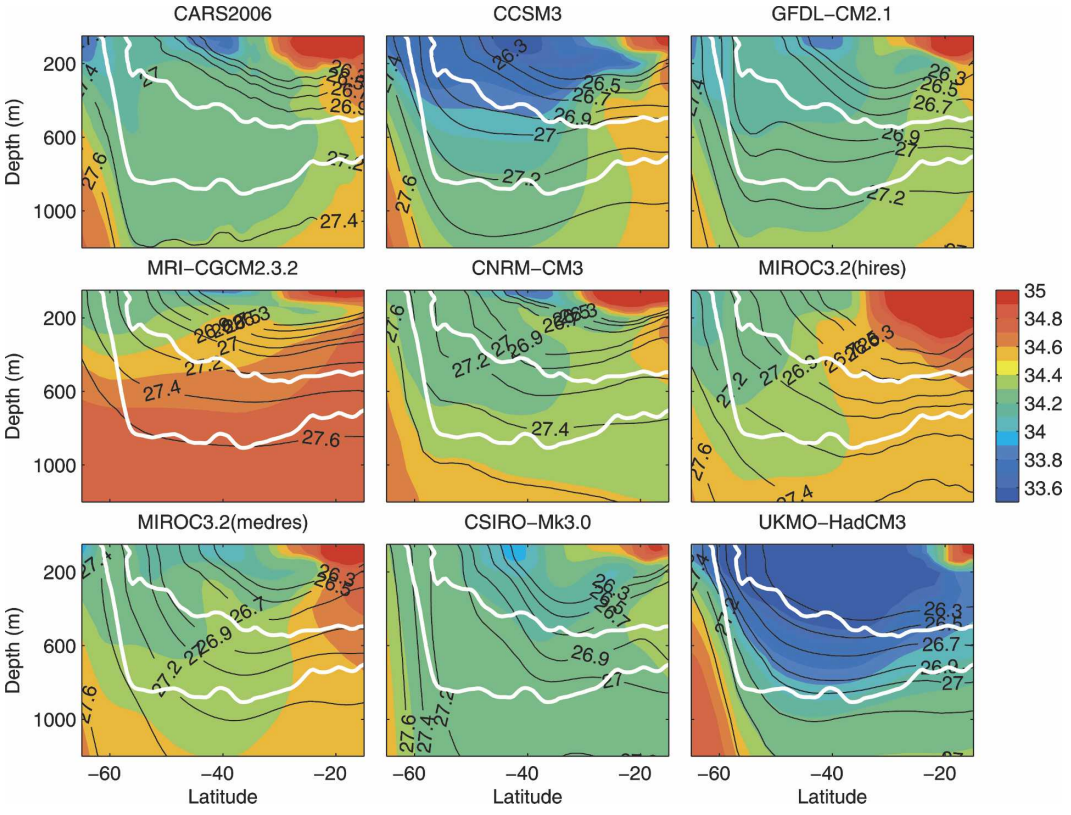

FIG. 10. Austral spring distribution of salinity (psu) in the eastern Pacific Ocean (90°W) from CARS2006 and eight climate models. The depth and latitudinal extent of the observed potential density surface that enclose the AAIW salinity minimum (bold white) are overlain on climate model salinity distribution. Also shown is the distribution of potential density (solid black).

larger than the corresponding values in the inverse model. Qualitatively, for all methods, the results do not change, and here we discuss the property transports based on the neutral density water mass definition as given in Sloyan and Rintoul (2001b). In this comparison, it must be kept in mind that error estimates by the inverse model are the formal errors of the minimization technique and may not represent true uncertainty in the data.

a. Atlantic Ocean

The inverse model estimates a net northward volume and temperature transport of 12.3 ± 0.6 ($\times 10^6$ m^3 s^{-1}) and 0.43 ± 0.03 PW of SAMW and AAIW across 12°S in the Atlantic Ocean (Fig. 11). In the inverse model, the volume transport is dominated by strong northward flow adjacent to Africa and broad weak northward flow in the interior Brazil Basin that is balanced by southward flow in the Angola Basin. The southward flow in the Angola Basin supports observations of a high-oxygen and low-salinity tongue extending eastward south of the equator (Suga and Talley 1995). At 12°S the net northward volume transport of the climate models varies between 8.7×10^6 (CCSM3) and 10.8×10^6 m^3 s^{-1}(CNRM-CM3), which are smaller than the inverse model estimate. Zonal structure of the climate-model simulated flow is different than in the inverse model. All models exhibit a broader [14 − 12 ($\times 10^6$ m^3 s^{-1})] northward flow near the South American coast relative to the inverse model (12.7×10^6 m^3 s^{-1}). In the interior of the Brazil Basin the climate models have a small southward flow and they do not resolve the eddy-like structure of the net southward flow in the Angola Basin. The northward temperature transport among the climate models ranges between 0.42 and 0.56 PW (Fig. 11), similar to or slightly larger than the inverse model estimate. Differences in the temperature of the SAMW and AAIW layer among the climate model and observations result in differences in the estimated layer temperature transport.

The northward flow of SAMW and AAIW across 12°S in the Atlantic Ocean principally balances the southward flow of NADW (Sloyan and Rintoul 2001a). The inverse model has southward transport of

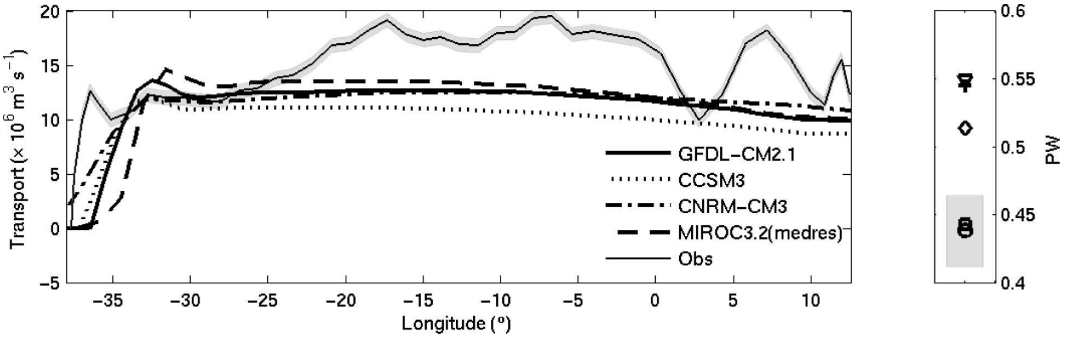

FIG. 11. (left) Comparison of the cumulative volume transport (Sv), across the Atlantic Ocean at 12°S, of SAMW and AAIW between the observation-based inverse model (thin line, circle) and four climate models: GFDL-CM2.1 (solid, diamond), CCSM3 (dotted, square), CNRM-CM3 (dot–dashed, triangle), and MIROC3.2(medres) (dashed, plus). (right) The SAMW and AAIW layer temperature transport (1 PW = 1×10^{15} W), relative to 0°C, for the inverse model and climate models. Gray shading is the formal error of the inverse model. Positive transport is northward.

18.0 ± 2.4 ($\times 10^6$ m^3 s^{-1}) of NADW, and the climate model maximum southward transport of the Atlantic overturning circulation varies between 15.7×10^6 (GFDL-CM2.1) and 10.7×10^6 m^3 s^{-1} [MIROC3.2(medres)]. In the inverse model the SAMW and AAIW northward transport provides 68% of the water required to balance the southward NADW transport. GFDL-CM2.1 and CCSM3 have a similar balance between their simulated SAMW and AAIW, and NADW transports of 63% and 71%, repectively, while CNRM-CM3 and MIROC3.2(medres) have a balance of 77% and 94%, respectively.

b. Pacific Ocean

The western boundary current of the South Pacific Ocean north of 30°S is found adjacent to Australia—the East Australian Current (EAC). The EAC separates from the Australian coast between 30° and 35°S, forming the Tasman Front that meanders eastward across the Tasman Sea in a series of semipermanent eddies, until a southward western boundary flow is reestablished adjacent to New Zealand—the East Auckland Current (Roemmich and Sutton 1998; Ridgway and Dunn 2003). The inverse model captures the complicated southward western boundary transport adjacent to Australia, across the Tasman Sea, and north of New Zealand (Fig. 12). In the SAMW and AAIW layer the southward flow at the western boundary and the broad northward flow in the interior of the gyre nearly balance, resulting in a small [3 ± 3 ($\times 10^6$ m^3 s^{-1})] net volume flux into the Pacific Ocean. [In the inverse model, much of the northward flow that balances the Indonesian Throughflow occurs within the lighter thermocline and surface water masses (Sloyan and Rintoul 2001a).]

All four climate models realistically simulate the longitudinal distribution of SAMW and AAIW volume transport across the Pacific Ocean (Fig. 12). The climate models, however, do not simulate the complicated circulation pattern in the Tasman Sea and north of New Zealand. In general, the model western boundary current is broader than observed and the EAC is stronger in all models, while north of New Zealand

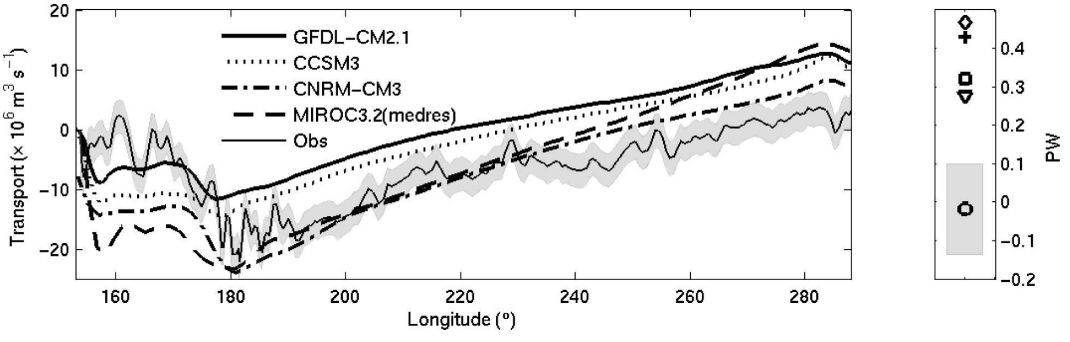

FIG. 12. As for Fig. 11, except for Pacific Ocean across 32°S.

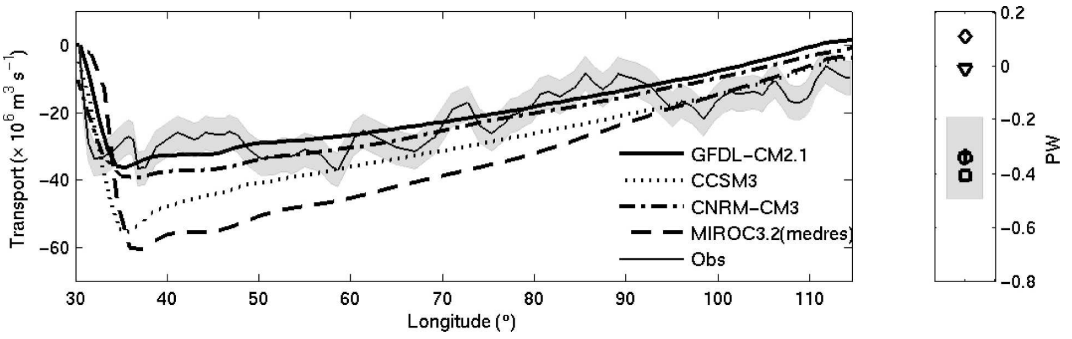

FIG. 13. As for Fig. 11, except for Indian Ocean across 32°S.

MIROC3.2(medres) and CNRM-CM3 slightly overestimate the net southward flow, and the GFDL-CM2.1 and CCSM3 models underestimate the transport. The coarse horizontal resolution and subgrid-scale isopycnal mixing schemes employed in many models result in an overly broad EAC and lack of transport detail in the Tasman Sea. Differences in the strength of the EAC at 32°S between the observation-based inverse model and among the climate models could be related to a number of factors including simulation of the correct position of the separation of the EAC from the coast and correct partition at the separation point between water flowing eastward with the Tasman Sea Front and water continuing southward with the EAC extension.

Comparisons between GFDL-CM2.0 and -CM2.1 show that, although both of these models correctly simulate the separation point of the EAC, the model versions differ in the partitioning of the transport between water that flows eastward in the Tasman Front and water that continues south in the EAC extension (Gnanadesikan et al. 2006). [In this study we use the GFDL-CM2.1 (Table 1).] CM2.1 shows better agreement with observations, while CM2.0 has a strong Tasman Front and little flow continuing southward in the extension. The difference between these two versions is explained by the position of the positive wind stress curl over the Pacific Ocean. For similar reasons, the MIROC3.2(medres) and CNRM-CM3 may overestimate the eastward volume transport associated with the Tasman Front and strength of the southward flow north of New Zealand.

In all climate models, the northward interior transport of SAMW and AAIW across 32°S into the Pacific Ocean is larger than the inverse-model transport estimate (Fig. 12). The GFDL-CM2.1 and CCSM3 interior northward transports, however, are only slightly larger than in the inverse model. In contrast, the CNRM-CM3 and MIROC3.2(medres), in the SAMW and AAIW layer, exhibit a much stronger northward interior transport than the inverse model. In these models the large southward transport at the western boundary is more than compensated by northward interior transport.

The inverse model estimates a small southward temperature transport of the SAMW and AAIW layer (Fig. 12). In all climate models, stronger than observed northward volume flux across 32°S leads to a northward temperature transport into the Pacific Ocean of between 0.28 and 0.49 PW. The rms isopycnal temperature error distribution (Fig. 4) is very similar for the GFDL-CM2.1, CNRM-CM3, CCSM3, and MIROC3.2(medres) and therefore differences in the model temperature transports are in principle explained by the differences in the layer volume transport.

c. Indian Ocean

In the southern Indian Ocean, the inverse model SAMW and AAIW layer circulation is dominated by the southward transport associated with the Agulhas Current that exceeds the northward transport in the central and eastern Indian Ocean (Fig. 13). The net southward volume transport of SAMW and AAIW of 10 ± 5 Sv ($1\ \text{Sv} \equiv 10^6\ \text{m}^3\ \text{s}^{-1}$) is balanced by northward flow of thermocline and surface water in the Pacific Ocean (Sloyan and Rintoul 2001a). The GFDL-CM2.1 and CNRM-CM3 simulated southward SAMW and AAIW volume flux in the Agulhas Current is slightly larger than that estimated by the inverse model, while in CCSM3 and MIROC3.2(medres) the southward transport is almost 100% greater than the inverse model transport. In the climate models the partially compensating northward volume transport in the central and eastern Indian Ocean is larger than the observation-based inverse model estimate, resulting in a model-simulated net volume flux across 32°S of between $-3.75 \times 10^6\ \text{m}^3\ \text{s}^{-1}$(CCSMS) and $1.5 \times 10^6\ \text{m}^3\ \text{s}^{-1}$(GFDL-CM2.1) (Fig. 13).

The inverse model estimates a southward temperature transport for the SAMW and AAIW layer across the Indian Ocean at 32°S. MIROC3.2(medres) and

CCSM3 have a southward temperature transport, while GFDL-CM2.1 and CNRM-CM3 have a small northward temperature transport. The difference in heat flux between the inverse model and climate models is mostly explained by the difference in volume fluxes across 32°S. It is coincidental that the MIROC3.2(medres) and CCSM3 simulated temperature transports agree with the inverse model estimate. In these models this is a balance between the southward volume transport in the Aguhlas Current and northward volume transport in the ocean interior. In contrast, the GFDL-CM2.1 and CNRM-CM3 northward temperature transports results from the large northward volume transport in the ocean interior.

6. Boundary forcing and impacts on SAMW and AAIW formation and subduction

Errors in SAMW and AAIW properties (temperature, salinity, density, and salinity potential vorticity minimum) indicate inadequate representation of processes that ventilate the Southern Ocean and mixed layer dynamics during the local winter, which have important consequences for the ocean heat, freshwater, and carbon budgets. It is also important that climate models correctly simulate the vertical position of the SAMW and AAIW core, as these water masses are suggested to strongly affect the depth of the main pycnocline and the meridional overturning circulation. Limited equatorward penetration of SAMW and AAIW suggests inadequate ventilation of the subsurface Southern Hemisphere gyres with significant impact on midlatitude primary production.

An observed decadal spinup of the South Pacific is suggested to be related to the intensification of the wind stress curl east of New Zealand (Roemmich et al. 2007). Therefore, by analogy, the stronger subtropical gyre circulation in the climate models relative to the inverse model estimate may be due to a bias in atmospheric wind stress curl. In many models the wind stress maximum and wind stress curl is broader than observed, resulting in stronger wind stress and wind stress curl over the midlatitude oceans than found in reanalysis products (Large and Danabasoglu 2006; Yeager et al. 2006; Russell et al. 2006). The latitudinal bias of the wind stress maximum is largest in the Pacific sector of the Southern Ocean (Fyfe and Saenko 2006).

The bias in the strength and position of the wind stress and wind stress curl in the climate models affects climate model simulation of the ACC (position and strength), position and strength of Ekman pumping and transport, and mechanical stirring. All of these processes have been suggested to be important in the formation of SAMW and AAIW. The error in size and position of the wind stress influences the property characteristics of SAMW and AAIW explicitly via northward Ekman transport of cold and fresh Antarctic Surface Water and wind-driven mechanical stirring of the upper-ocean water column. The correct position of the wind stress over the Southern Ocean, which for most regions of the Southern Ocean determines the position of the ACC, may also feed back onto the magnitude and spatial patterns of the air–sea buoyancy (heat and freshwater) fluxes. Climate models that simulate an equatorward bias in the position of the ACC may potentially distort the air–sea buoyancy fluxes over the SAMW and AAIW formation regions. We note that in some regions the position of the ACC is topographically constrained. However, our ability to assess the climate model simulation of Southern Ocean air–sea buoyancy fluxes and wind stress is severely limited by the lack of appropriate long-term observations.

The strength and position of the wind stress varies with latitude over the Southern Ocean. The strongest wind stress is over the Indian sector of the Southern Ocean, with a maximum centered near 50°S, while in the Pacific sector the magnitude of the wind stress decreases and the maximum shifts southward to approximately 55°S. The wind stress of the climate models also reflects this zonal variation in both strength and position (Fyfe and Saenko 2006). Fyfe and Saenko show a large variation in the position of the wind stress in the Pacific sector of the Southern Ocean for a group of climate models also considered in this study. The difference in the wind stress (position and strength) among the climate models and its influence on formation of SAMW and AAIW may explain the differences among the models' simulation of these water masses. Previous studies have shown that a southward shift in the wind stress, of constant strength, results in a freshening and increased formation of AAIW and cooling of SAMW (Oke and England 2004).

Another potentially important source of error in ocean models is inadequate representation of subgrid mixing processes in the Southern Ocean. Evaluation of the performance of various parameterization schemes employed by these climate models is beyond the scope of this study. We can, however, speculate on the potential importance of these processes for the formation and circulation of SAMW and AAIW masses. For example, realistic representation of the wind-induced turbulent mixing is crucial for adequate simulation of the mixed layer (Large et al. 1994) and SAMW pycnostad in the Southern Ocean. High-frequency variability in the wind forcing also plays an important role in mixed layer dynamics (Kamemkovich 2005). The fact that the model-

simulated mixed layer depth and thickness of the SAMW pycnostad are generally underestimated suggests that intensity of both mixing and atmospheric storm intensity may be underestimated by the climate models.

Adequate representation of mesoscale eddies in models represents one of the most long-standing challenges in physical oceanography. All parameterization methods are criticized for their low skill in capturing properties of actual eddy fluxes (Nakamura and Chao 2000; Roberts and Marshall 2000). At the same time, mesoscale eddies are widely believed to play a central role in maintaining the stratification in the ACC (Marshall and Radko 2003). Significant errors in isopycnal depth in climate models can therefore be caused by inadequate representation of eddy transport. For example, too weak eddies would result in overly steep isopycnals, as mesoscale eddies are generally believed to flatten isopycnal surfaces and vice versa. Effects of high-latitude eddies are not limited to the Southern Ocean but project on the adjacent ocean basins with the maximum effect at intermediate-water depths (Kamenkovich and Sarachik 2004). Improvements to the eddy parameterization schemes and/or development of eddy-resolving climate simulations is therefore a next major step in climate modeling.

In individual climate models there are regional difference in the "goodness" of the simulation of SAMW and AAIW. In general, models best simulate the isopycnal temperature and salinity of SAMW and AAIW in the eastern Pacific Ocean, while larger errors are found in the Indian Ocean and western Pacific Ocean. These regional differences in the model simulation of SAMW and AAIW raise interesting questions concerning both our understanding of the processes leading to the formation of these water masses at the different formation sites and the spatial variability in the relative role of the processes involved in the formation of SAMW and AAIW. The large isopycnal temperature and salinity errors at the western boundary of the Atlantic, Indian, and Pacific Oceans most likely results from the inability of the climate models to correctly simulate the complicated western boundary dynamics (Large and Danabasoglu 2006; Gnanadesikan et al. 2006) and water mass interaction between the subtropical gyres and Southern Ocean.

The limited equatorward extent of SAMW and AAIW low potential vorticity and salinity minimum, respectively, suggests that the climate models are, at midlatitudes, overly diffusive. The importance of diapycnal mixing in ocean circulation has been discussed in numerous studies [see review of Wunsch and Ferrari (2004)]. Together with the Southern Ocean eddies, vertical mixing plays a central role in controlling ocean stratification and oceanic heat transport (Gnanadesikan 1999; Gnanadesikan et al. 2003). Another, more immediate effect of diapycnal diffusion on the water mass properties is the cross-isopycnal erosion of characteristic properties. Poor conservation of the model-simulated AAIW salinity minimum layer north of 40°S provides evidence of overly large midlatitude diapycnal mixing in the climate models. Most climate models still employ values of vertical diffusion that are larger than those suggested by direct measurements in the midlatitude oceans (Ledwell et al. 1993). In addition, the advection and parameterization schemes still lead to significant spurious numerical diffusion (Griffies et al. 2000). This type of diapycnal mixing is very difficult to control in z coordinate models, even at very high resolution. It is clear that further advances in modeling and controlling diapycnal mixing are needed to eliminate this source of error.

Isopycnal depth errors of SAMW and AAIW are found in the subtropical gyres of the Atlantic, Indian, and Pacific Oceans. South of 35°S the rms isopycnal depth error is due to the climate models producing the SAMW pycnostad at lighter than observed densities, while north of 35°S the rms isopycnal depth error is due to a too warm upper ($\leq$600 m) ocean. In the Southern Hemisphere, temperature and salinity errors at the eastern boundary of the Pacific and Atlantic Oceans have been shown to have large-scale subsurface impacts in the respective subtropical gyres (Large and Danabasoglu 2006). Errors in the eastern boundaries are due to both local atmospheric forcing and ocean upwelling. This study finds that errors at the western and eastern boundaries of the subtropical oceans also impact the depth at which SAMW and AAIW circulate within the gyres. This error may significantly impact an assessment of SAMW and AAIW variability and change, under IPCC climate scenarios, on the nutrient cycle and primary production in the subtropical and tropical oceans.

7. Conclusions

This study evaluates the simulation of SAMW and AAIW in eight IPCC climate models relative to the CARS2006 climatology of the Southern Hemisphere oceans. The climate model drift north of the SAMW and AAIW formation region, which was not removed in this analysis, is 5 times smaller than rms property errors between the climate models and observations. The study shows that the climate models, except for UKMO-HadCM3, CSIRO-Mk3.0, and MRI-CGCM2.3.2, provide a reasonable simulation of the isopycnal tempera-

ture and salinity properties of SAMW and AAIW in their formation region. The climate models also simulate reasonably well the potential vorticity minimum layer associated with SAMW and the salinity minimum of the layer associated with AAIW in the Southern Ocean. The simulated salinity minimum is at the observed density, while the simulated potential vorticity minimum is at lighter densities than observed. All models display a limited equatorward extension of the potential vorticity and salinity minimum of SAMW and AAIW. This suggests that, in general, north of 40°S the climate models are too diffusive.

The SAMW potential vorticity minimum layer is generally thinner and less dense than observed, particularly in the Indian Ocean sector of the Southern Ocean. It is suggested that the limited vertical extent of the potential vorticity minimum and its lighter density in the climate models may be explained by processes that determine the formation and properties of SAMW. These include the overly strong recirculation of warm and salty subtropical water at the western boundary of the Indian and Pacific Oceans, the northward displacements of the wind stress maximum in the Southern Ocean, and inadequate representation of subgrid-scale mixing processes. A combination of the processes involved in the formation of SAMW influenced by the wind and buoyancy forcing may explain the low density bias of SAMW in the climate models. A low-salinity tongue commonly associated with AAIW is clearly seen in all model simulations. The depth and isopycnal horizon of AAIW is well simulated in many climate models and has a reasonable meridional extent in CCSM3, GFDL-CM2.1, CNRM-CM3, and both MIROC models. Simulation of SAMW and AAIW in the Pacific is generally more realistic, relative to observations.

SAMW and AAIW meridional volume and temperature transport across 12°S in the Atlantic and 32°S in the Indian and Pacific Oceans of CCSM3, GFDL-CM2.1, CNRN, and MIROC3.2(medres) were compared to estimates from an observation-based inverse model. The climate models simulate the subtropical gyre circulation pattern, and the circulation of SAMW and AAIW is realistic when compared to the inverse model. The climate models, in the Indian and Pacific Oceans, overestimate both the northward and southward components of the flow pattern. The most likely cause of the stronger gyre circulation in the climate models, relative to the inverse model, is the northward displacement wind stress curl, which results in stronger wind forcing between 45° and 30°S.

We note that some climate models have undergone further development since submission to the IPCC Fourth Assessment Report. A known bias in the hydrological cycle of the UKMO-HadCM3 severely impacts the model simulation of SAMW and AAIW. The UKMO-HadCM3 is now superseded by the Hadley Centre Global Environmental Model (HadGEM). Many of the problems identified with SAMW and AAIW simulation in UKMO-HadCM3 may be reduced or removed in HadGEM. This study notes that, although the CSIRO-Mk3.0 rms isopycnal temperature and salinity errors are small among the climate models when compared to CARS2006, the model has overly vigorous vertical mixing surrounding the ACC. This is due to a low choice of the Gent–McWilliams κ (to achieve better simulation of the North Atlantic thermohaline circulation), which results in a number of deficiencies in the simulation of the Southern Ocean. Further development of the CSIRO-Mk3.0 model has improved the simulation of the Southern Ocean, including more realistic mixed layer depths and stratification (S. O'Farrell and A. Hirst 2006, personal communication).

This study is the first step in a thorough analysis of climate model simulations of Southern Ocean water masses, involving comparisons with observations and among the models. Significant developments in the climate models over recent years have resulted in a reasonable simulation of SAMW and AAIW in many models. Of particular interest is the generally better simulation of SAMW and AAIW in the southeast Pacific than in the Indian sector of the Southern Ocean. Although beyond the scope of this study, understanding this difference may help unravel the relative importance of the many processes involved in SAMW and AAIW water mass formation at and between these two formation regions.

Acknowledgments. This paper is a contribution to the CSIRO Climate Change Research Program and the CSIRO Wealth from Oceans Flagship. BMS was partly funded by the Australian Climate Change Science Program. IVK was funded by NSF and DOE as a Climate Model Evaluation Project (CMEP) grant (NSF ATM 0447034) under the U.S. CLIVAR Program (http://www.usclivar.org/index.html), and by NSF through the Office of Polar Programs under Grant 0126208. We thank the modeling groups for providing their data for analysis, the Program for Climate Model Diagnosis and Intercomparison (PCMDI) for collecting and archiving the model output, and the JSC/CLIVAR Working Group on Coupled Modeling (WGCM) for organizing the model data analysis activity. The multi-model data archive is supported by the Office of Science, U.S. Department of Energy.

REFERENCES

Arbic, B. K., and W. B. Owens, 2001: Climatic warming of Atlantic intermediate waters. *J. Climate,* **14,** 4091–4108.

Banks, H., and R. Wood, 2002: Where to look for anthropogenic climate change in the ocean. *J. Climate,* **15,** 879–891.

——, and N. L. Bindoff, 2003: Comparison of observed temperature and salinity changes in the Indo–Pacific with results from the coupled climate model HadCM3: Processes and mechanisms. *J. Climate,* **16,** 156–166.

Bindoff, N. L., and J. A. Church, 1992: Warming of the water column in the south–west Pacific Ocean. *Nature,* **357,** 59–62.

——, and T. J. McDougall, 1994: Diagnosing climate change and ocean ventilation using hydrographic data. *J. Phys. Oceanogr.,* **24,** 1137–1152.

——, and ——, 2000: Decadal changes along an Indian Ocean section at 32°S and their interpretation. *J. Phys. Oceanogr.,* **30,** 1207–1222.

Bryden, H. L., E. L. McDonagh, and B. A. King, 2003: Changes in ocean water mass properties: Oscillations or trends? *Science,* **300,** 2086–2088.

Dunn, J. R., and K. R. Ridgway, 2002: Mapping ocean properties in regions of complex topography. *Deep-Sea Res. I,* **49,** 591–604.

Fyfe, J. C., and O. A. Saenko, 2006: Simulated changes in the extratropical southern hemisphere winds and currents. *Geophys. Res. Lett.,* **33,** L06701, doi:10.1029/2005GL025332.

Gent, P. R., and J. C. McWilliams, 1990: Isopycnal mixing in ocean circulation models. *J. Phys. Oceanogr.,* **20,** 150–155.

Gille, S. T., 2002: Warming of the Southern Ocean since the 1950s. *Science,* **295,** 1275–1277.

Gnanadesikan, A., 1999: A simple predictive model for the structure of the oceanic pycnocline. *Science,* **283,** 2077–2079.

——, B. L. Samuels, and R. D. Slater, 2003: Sensitivity of water mass transformation and heat transport to subgridscale mixing in coarse-resolution ocean models. *Geophys. Res. Lett.,* **30,** 1967, doi:10.1029/2003GL018036.

——, and Coauthors, 2006: GFDL's CM2 global coupled climate models. Part II: The baseline ocean simulation. *J. Climate,* **19,** 675–697.

Goodman, P. J., 2001: Thermohaline adjustment and advection in an OGCM. *J. Phys. Oceanogr.,* **31,** 1477–1497.

Gordon, A. L., 1986: Interocean exchange of thermocline water. *J. Geophys. Res.,* **91,** 5037–5046.

——, 2001: Interocean exchange. *Ocean Circulation and Climate,* G. Siedler, J. Church, and J. Gould, Eds., Academic Press, 303–314.

Griffies, S. M., R. Pacanowski, and R. Hallberg, 2000: Spurious diapycnal mixing associated with advection in a *z*-coordinate ocean model. *Mon. Wea. Rev.,* **128,** 538–564.

Hanawa, K., and L. D. Talley, 2001: Mode waters. *Ocean Circulation and Climate,* G. Siedler, J. Church, and J. Gould, Eds., Academic Press, 373–386.

Johnson, G. C., and A. H. Orsi, 1997: Southwest Pacific Ocean water-mass changes between 1968/69 and 1990/91. *J. Climate,* **10,** 306–316.

Kamenkovich, I. V., 2005: Role of daily surface forcing in setting the temperature and mixed layer structure of the Southern Ocean. *J. Geophys. Res.,* **110,** C07006, doi:10.1029/2004JC002610.

——, and E. S. Sarachik, 2004: Mechanisms controlling the sensitivity of the Atlantic thermohaline circulation to the parameterization of eddy transports in ocean GCMs. *J. Phys. Oceanogr.,* **34,** 1628–1647.

——, A. Sokolov, and P. H. Stone, 2002: An efficient climate model with a 3D ocean and statistical-dynamical atmosphere. *Climate Dyn.,* **19,** 585–598.

Keeling, R. F., 2002: On the freshwater forcing of the thermohaline circulation in the limit of low diapycnal mixing. *J. Geophys. Res.,* **107,** 3077, doi:10.1029/2000JC000685.

Kraus, E. B., and J. S. Turner, 1967: A one-dimensional model of the seasonal thermocline. 2. The general theory and its consequences. *Tellus,* **19,** 98–106.

Large, W. G., and G. Danabasoglu, 2006: Attribution and impacts of upper-ocean biases in CCSM3. *J. Climate,* **19,** 2325–2346.

——, J. C. McWilliams, and S. C. Doney, 1994: Oceanic vertical mixing: A review and a model with a nonlocal boundary layer parameterization. *Rev. Geophys.,* **32,** 363–403.

Ledwell, J. R., A. J. Watson, and C. S. Law, 1993: Evidence for slow mixing across the pycnocline from an open-ocean tracer-release experiment. *Nature,* **364,** 701–703.

Marshall, J., and T. Radko, 2003: Residual-mean solutions for the Antarctic Circumpolar Current and its associated overturning circulation. *J. Phys. Oceanogr.,* **33,** 2341–2354.

McCartney, M. S., 1977: *Subantarctic Mode Water. A Voyage of Discovery: George Deacon 70th Anniversary Volume,* M. V. Angel, Ed., Pergamon, 103–119.

——, 1982: The subtropical recirculation of mode waters. *J. Mar. Res.,* **40,** 427–464.

Mellor, G. L., and T. Yamada, 1982: Development of a turbulence closure model for geophysical fluid problems. *Rev. Geophys.,* **20,** 851–875.

Nakamura, M., and Y. Chao, 2000: On the eddy isopycnal thickness diffusivity of the Gent–McWilliams subgrid mixing parameterization. *J. Climate,* **13,** 502–510.

Oke, P. R., and M. H. England, 2004: Oceanic response to changes in the latitude of the Southern Hemisphere subpolar westerly winds. *J. Climate,* **17,** 1040–1054.

Orsi, A. H., T. Whitworth III, and W. D. Nowlin Jr., 1995: On the meridional extent and fronts of the Antarctic circumpolar current. *Deep-Sea Res. I,* **42,** 641–673.

Pardaens, A. K., H. T. Banks, J. M. Gregory, and P. R. Rowntree, 2003: Freshwater transports in HadCM3. *Climate Dyn.,* **21,** 177–195.

Piola, A. R., and D. T. Georgi, 1982: Circumpolar properties of Antarctic intermediate water and subantarctic mode water. *Deep-Sea Res.,* **29,** 687–711.

——, and A. L. Gordon, 1989: Intermediate water in the southwestern South Atlantic. *Deep-Sea Res.,* **36,** 1–16.

Price, J. F., R. A. Weller, and R. Pinkel, 1986: Diurnal cycling: Observations and models of the upper ocean response to diurnal heating, cooling and wind mixing. *J. Geophys. Res.,* **91,** 8411–8427.

Ribbe, J., 1999: On wind-driven mid-latitude convection in ocean general circulation models. *Tellus,* **51A,** 517–525.

——, 2001: Intermediate water mass production controlled by southern hemisphere winds. *Geophys. Res. Lett.,* **28,** 535–538.

Ridgway, K. R., and J. R. Dunn, 2003: Mesocale structure of the mean East Australian current system and its relationship with topography. *Prog. Oceanogr.,* **56,** 189–222.

——, ——, and J. L. Wilkin, 2002: Ocean interpolation by four-dimensional weighted least squares—Application to the waters around Australasia. *J. Atmos. Oceanic Technol.,* **19,** 1357–1375.

Rintoul, S. R., 1991: South Atlantic interbasin exchange. *J. Geophys. Res.,* **96,** 2675–2692.

——, and M. H. England, 2002: Ekman transport dominates local air–sea fluxes in driving variability of subantarctic mode water. *J. Phys. Oceanogr.,* **32,** 1308–1321.

Roberts, M., and D. Marshall, 2000: On the validity of downgradient eddy closures in ocean models. *J. Geophys. Res.,* **105,** 28 613–28 627.

Roemmich, D., and P. Sutton, 1998: The mean and variability of ocean circulation past northern New Zealand: Determining the representativeness of hydrographic climatologies. *J. Geophys. Res.,* **103,** 13 041–13 054.

——, J. Gilson, R. Davis, P. Sutton, S. Wijffels, and S. Riser, 2007: Decadal spinup of the South Pacific subtropical gyre. *J. Phys. Oceanogr.,* **37,** 162–173.

Russell, J. L., R. J. Stouffer, and K. W. Dixon, 2006: Intercomparison of the Southern Ocean circulations in IPCC coupled model control simulations. *J. Climate,* **19,** 4560–4575.

Saenko, O. A., A. J. Weaver, and J. M. Gregory, 2003: On the link between the two modes of the ocean thermohaline circulation and the formation of global-scale water masses. *J. Climate,* **16,** 2797–2801.

Santoso, A., and M. H. England, 2004: Antarctic intermediate water circulation and variability in a coupled climate model. *J. Phys. Oceanogr.,* **34,** 2160–2179.

Sarmiento, J. L., N. Gruber, M. A. Brzezinski, and J. P. Dunne, 2004: High-latitude controls of thermocline nutrients and low latitude biological productivity. *Nature,* **427,** 56–60.

Saunders, P. M., and B. A. King, 1995: Oceanic fluxes on the WOCE A11 section. *J. Phys. Oceanogr.,* **25,** 1942–1958.

Schmitz, W. J., Jr., 1996: On the world ocean circulation. Volume II: The Pacific and Indian Oceans—A global update. Tech. Rep. WHOI-96-08, 237 pp.

Sloyan, B. M., and S. R. Rintoul, 2001a: Circulation, renewal, and modification of Antarctic mode and intermediate water. *J. Phys. Oceanogr.,* **31,** 1005–1030.

——, and ——, 2001b: The Southern Ocean limb of the global deep overturning circulation. *J. Phys. Oceanogr.,* **31,** 143–173.

Suga, T., and L. D. Talley, 1995: Antarctic intermediate water circulation in the tropical and subtropical South Atlantic. *J. Geophys. Res.,* **100,** 13 441–13 454.

Treguier, A. M., O. Boebel, B. Barnier, and G. Madec, 2003: Agulhas eddy fluxes in a 1/6° Atlantic model. *Deep-Sea Res. II,* **50,** 251–280.

Wang, X., P. H. Stone, and J. Marotzke, 1999: Global thermohaline circulation. Part I: Sensitivity to atmospheric moisture transport. *J. Climate,* **12,** 71–82.

Wilson, S. G., 2000: How ocean vertical mixing and accumulation of warm surface water influence the "sharpness" of the equatorial thermocline. *J. Climate,* **13,** 3638–3656.

Wong, A. P. S., N. L. Bindoff, and J. A. Church, 1999: Large-scale freshening of intermediate waters in the Pacific and Indian Oceans. *Nature,* **400,** 440–443.

Wunsch, C., and R. Ferrari, 2004: Vertical mixing, energy, and the general circulation of the oceans. *Annu. Rev. Fluid Mech.,* **36,** 281–314.

Yeager, S. G., C. A. Shields, W. G. Large, and J. J. Hack, 2006: The low-resolution CCSM3. *J. Climate,* **19,** 2545–2566.